Research Article

Evaluation of an advanced model reference sliding mode control method for cardiac assist device using a numerical model

Mohsen Bakouri[1,2] ✉

[1]Department of Medical Equipment Technology, College of Applied Medical Science, Majmaah University, Address, Majmaah City, Saudi Arabia
[2]Department of Physics, College of Science, Sebha University, Address, Traghen City, Libya
✉ E-mail: m.bakouri@mu.edu.sa

Abstract: In this study, the physiological control algorithm using sliding mode control method is implemented to track the reference input signal. The controller is developed using feed-forward part, reference model, and steady-state flow estimator. The proposed control method is evaluated using a dynamic heart-pump interaction model incorporating descriptions of the cardiovascular system – rotary blood pump. The immediate response of the controller to preload as well as afterload was studied. Stability and feasibility of the control system were demonstrated through the tests. The results showed that the present controller, which allows the left ventricular to automatically adjust to the right ventricular output, reduces the risk of suction.

1 Introduction

The incidence of advanced heart failure (HF) continues to double every 10 years [1]. Whilst medical and surgical advances continue to occur, an ever-increasing number of patients are listed for cardiac transplantation each year. However, the number of donor organs remains limited and the short-term treatment of HF disease using continuous intravenous inotrope support may improve symptoms but may worsen mortality [2, 3]. Therefore, lack of effective pharmaceutical and transplant options has driven HF therapy to look toward mechanical pumping assistance [4].

The mechanical circulatory support type implantable rotary blood pumps (IRBPs) represent a major advantage in the management of end stage HF [3, 5]. However, the morbidity and mortality associated with their use are still unacceptably high. The interaction between native failing heart and IRBP is poorly characterised and is associated with both morbidity and preventable mortality [6]. A complete understanding of the physiological and anatomical interaction between IRBPs and the diseased ventricles will facilitate strategies to optimise the hearts dynamic geometry, promote myocardial recovery and develop diagnostic pathways to optimise IRBP management [7]. Translating this research into practice will optimise the potential of such poorly managed devices, enabling improved lifestyle and mortality of patients.

One of the challenges is the wide range of degrees of HF that need to be accommodated, poor ventricular function with virtually no pulsatility to accurate ventricular function where significant aortic valve flow exists [4]. Some observers initially claimed that the flatter pressure differential/flow characteristics of centrifugal devices at a fixed average speed offered an inherent flow adaptation for different levels of preload. However, some researchers show these rotary devices to be preload insensitive meaning that additional sensors are required to give these systems a natural Frank–Starling behaviour [8]. Most commercial rotary ventricular assist devices (VADs) currently operate at a fixed speed which is set and adjusted by an expert clinician. Many researchers have reported bench-based (mock loop) experiments, e.g. Giridharan *et al.* [9] who purports that regulation of VAD head pressure provides physiological control. Some rotary VADs do have controllers which can be adjusted for different activity levels. Flow maker [10] allows patients to manually switch to three different speeds set by an expert clinician which correspond with low, medium, and high levels of activity.

In this field, the traditional control strategy, which maintains a constant pump speed, demonstrates a limited degree of adaptability to cardiac demand and clinical conditions of the heart. For instance, We *et al.* [11] designed physiological control algorithm using an optimal proportional–integral (PI) controller to maintain aortic pressure and prevent suction. This algorithm allowed for an automatic response to the changing metabolic demands of the circulatory system. However, maintaining aortic pressure at a constant value may increase the risk of suction under low systemic vascular resistance/blood volume conditions, while producing lower than optimal cardiac output under higher blood volume conditions. Furthermore, Choi *et al.* [12] developed a physiological controller to optimise the blood flow using the fuzzy logic controller to prevent ventricular collapse. The main drawback related to this control strategy is the selection of a suitable pump flow level.

To overcome the issue, the novel method of an advanced physiological control algorithm is proposed and implemented to drive a pump rotational speed in accordance with the body metabolic demand. The proposed method is designed using the reference model of sliding mode control (SMC) method where the sliding surface is implemented using error states of the original model and designed the reference model [13].

2 Methods

2.1 VAD model

In order to simulate a wide range of cardiovascular states and pump operating conditions, a software model of the cardiovascular system (CVS) together with the left VAD (LVAD) was used to evaluate the control strategy. The model has been developed based on experimental measurements obtained from five greyhounds implanted with an IRBP, over a wide range of operating conditions, including variations in cardiac contractility, systemic vascular resistance and total circulatory volume [14]. Least square parameter estimation methods were utilised to fit a subset of model parameters in order to achieve better agreement with the experimental data and to evaluate the robustness and validity of the model under various operating conditions.

2.2 Flow estimator model

The control method was developed using non-invasive average pulsatile pump flow estimator model. The estimator model consisting of two auto-regressive (ARX) model. The first proposed
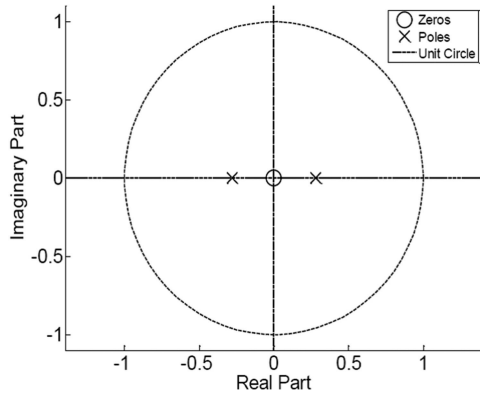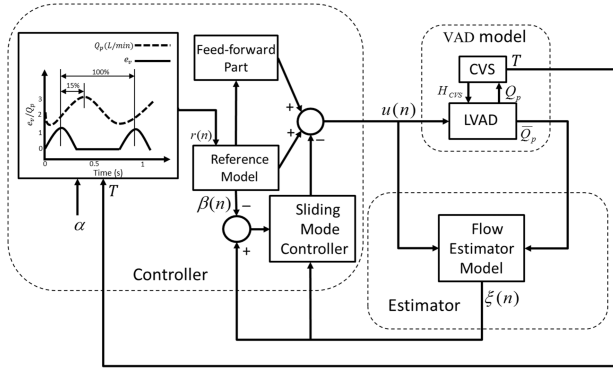
Fig. 1 *Poles-zeros of the system model*

Fig. 2 *Control system with the reference model, estimator and VAD model. r(n), reference flow; u(n), control input; H_{cvs}, differential pressure; CVS, cardiovascular system; Q_p, instantaneous pump flow; $\overline{Q}_p$, mean pump flow; e_v, elastance function; T, heart period; α, constant*
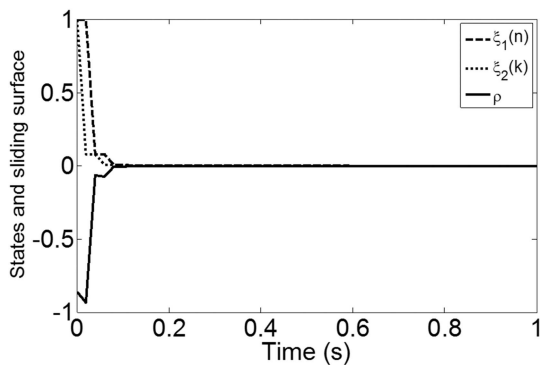

Fig. 3 *System response*

ARX model represents the relation between average pulsatility index of pump rotational speed and average pulse-width modulation signal as an input signal to estimate. Then, the second proposed ARX model represents the average pulsatile flow as estimated from. The performance of the model was carefully validated using different values of hemodynamic parameters including systemic vascular resistance, total blood volume and the left and right ventricular contractility. In addition, the stability of this model is studied and Fig. 1 indicates that the pole-zeros of the model estimator are located within the unit circle. A detailed description of the model, as well as parameter values, can be obtained from [15].

2.3 VAD control strategy

In the proposed method, we considered control system implantation in combination with the estimator and VAD model as shown in Fig. 2. The controller is designed to achieve that the flow error tends to zero ($e \rightarrow 0$) as the time tends to infinity ($t \rightarrow \infty$). Therefore, the reference model is designed as a part to drive the

control system. This reference model is used as a part of the SMC approach to control the reference pump flow. The reference pump flow is carefully designed using the preload (end diastolic function) in terms of left atrial filling (end systolic volume).

To achieve a physiological demand, the time varying of elastance function (e_v) at end systolic period is considered. Therefore, (e_v) is used where the maximum of this function has represented the end systolic period and the phase shift of 15% for sinusoidal reference pump flow is known as zero at the peak value of pump flow. Thus, the reference input signal is chosen as $r(n) = \alpha + \beta \sin(2\pi t/T + \gamma)$ where α, β and γ are constants, $\alpha > \beta$, while T is the heart period.

2.4 Controller design

The estimator model is identified by ARX model where the mathematical equation of this model is considered as

$$\xi(n + 1) = A\xi(n) + \Delta A\xi(n) + Bu(n) + \eta(n)$$
$$\varphi(n) = C\xi(n) \tag{1}$$

where ξ is the state of estimator model, u is the control signal, ΔA is estimator parameter variation, $\eta(n)$ is the system noise and A, B and C are model matrices.

Assume the corresponding reference model is given as

$$\beta(n + 1) = A_r\beta(n) + B_r r(n) \tag{2}$$

where β is the state vector, r is an input signal, A_r and B_r are model reference matrices.

The controller is designed and implemented based on the error tracking of states [16]. Therefore, if we define this error difference between plant and model sate response as

$$e(n) = \xi(n) - \beta(n) \tag{3}$$

$$e(n + 1) = \xi(n + 1) - \beta(n + 1) \tag{4}$$

by updating the previous equation, we can obtain

$$e(n + 1) = A\xi(n) + \Delta A\xi(n) + Bu(n) + \eta(n)$$
$$- A_r\beta(n) - B_r r(n) \tag{5}$$

manipulating (5) with the term of $A_r\xi(n)$ yields

$$e(n + 1) = A\xi(n) + \Delta A\xi(n) - A_r\xi(n) + A_r\xi(n)$$
$$+ Bu(n) + \eta(n) - A_r\beta(n) - B_r r(n) \tag{6}$$

and by re-arranging (6), we can write

$$e(n + 1) = A_r e(n) + (A - A_r)\xi(n) + \Delta A\xi(n)$$
$$+ Bu(n) + \eta(n) - B_r r(n) \tag{7}$$

If we define the sliding surface as

$$\xi(n) = \rho e(n) \tag{8}$$

$$\xi(n + 1) = \rho e(n + 1) \tag{9}$$

where ρ is a constant vector and known as a switching function. This vector is designed to guarantee that $\xi(n)$ is asymptotically stable [17]. Fig. 3 shows the convergence performance of the state variables $\xi_1(n)$ and $\xi_2(n)$ as they move on the switching plane.

In this method, to achieve strong reachability [18] we propose the following reaching law as:

$$\xi(n + 1) = (1 - \tau T)\xi(n) - \epsilon T \text{sign}(\xi(n)) \tag{10}$$

from (7), (9) and (10) we can obtain

IET Syst. Biol., 2018, Vol. 12 Iss. 2, pp. 68-72

69

$$(1 - \tau T)\xi(n) - \epsilon T\text{sign}(\xi(n))$$
$$= \boldsymbol{\rho}(\boldsymbol{A}_r e(n) + (\boldsymbol{A} - \boldsymbol{A}_r)\xi(n) + \Delta\boldsymbol{A}\xi(n) \qquad (11)$$
$$+ \boldsymbol{B}u(n) + \eta(n) - \boldsymbol{B}_r r(n))$$

by solving the above equation for $u(n)$ yields

$$u(n) = -(\boldsymbol{\rho B})^{-1}(\boldsymbol{\rho A}_r e(n) + \boldsymbol{\rho}(\boldsymbol{A} - \boldsymbol{A}_r)\xi(n)$$
$$-\boldsymbol{\rho B}_r r(n) - (1 - \tau T)\xi(n) + \epsilon T\text{sign}(\xi(n))) \qquad (12)$$
$$-(\boldsymbol{\rho B})^{-1}(\boldsymbol{\rho}\Delta\boldsymbol{A}\xi(n) + \boldsymbol{\rho}\eta(n))$$

As $\Delta\boldsymbol{A}$ and $\eta(n)$ are unknown, we may assume that the upper and lower bounds of the value $(\boldsymbol{\rho}\Delta\boldsymbol{A}\xi(n) + \boldsymbol{\rho}\eta(n))$ are known

$$-\alpha T < (\boldsymbol{\rho}\Delta\boldsymbol{A}\xi(n) + \boldsymbol{\rho}\eta(n)) < \alpha T \qquad (13)$$

then the control algorithm can be given as

$$u(n) = -(\boldsymbol{\rho B})^{-1}(\boldsymbol{\rho A}_r e(n) + \boldsymbol{\rho}(\boldsymbol{A} - \boldsymbol{A}_r)\xi(n)$$
$$-\boldsymbol{\rho B}_r r(n) - (1 - \tau T)\xi(n) + \epsilon T\text{sign}(\xi(n))) \qquad (14)$$
$$-(\boldsymbol{\rho B})^{-1}\alpha T\text{sign}(\xi(n))$$

Now consider the control law is structured as

$$u(n) = u_1(n) + u_2(n) = u_l(n) + u_{nl}(n) + u_2(n) \qquad (15)$$

here, the linear part is known as

$$u_l(n) = -(\boldsymbol{\rho B})^{-1}(\boldsymbol{\rho A}_r e(n)) \qquad (16)$$

and the non-linear part is known as

$$u_{nl}(n) = -(\boldsymbol{\rho B})^{-1}(-1(1 - \tau T)\xi(n) + \epsilon T\text{sign}(\xi(n)))$$
$$+ \alpha T\text{sign}(\xi(n)) \qquad (17)$$

To understand $u_2(n)$ better let us consider the following theorem with non-proof in linear algebra [16].

Theorem 1: For the following system denoted by:

$$RX = Y$$

has only one solution if and only if

$$rank[RY] = rank[R]$$

here, if the following conditions hold:

$$rank[\boldsymbol{BA}_r - \boldsymbol{A}] = rank[\boldsymbol{B}] \qquad (18)$$

$$rank[\boldsymbol{BB}_r] = rank[\boldsymbol{B}] \qquad (19)$$

then there are existing terms which are ($\boldsymbol{F}$) and ($\boldsymbol{G}$) can be written as

$$\boldsymbol{A}_r = \boldsymbol{A} + \boldsymbol{BF} \qquad (20)$$

$$\boldsymbol{B}_r = \boldsymbol{BG} \qquad (21)$$

it also follows that the control law $u_2(n)$ can be expressed as

$$u_2(n) = \boldsymbol{F}\xi(n) + \boldsymbol{G}r(n) \qquad (22)$$

where $\boldsymbol{G}$ and $\boldsymbol{F}$ are known as feed-forward gain and state feedback matrices, respectively. The feed-forward part can be obtained as

$$\boldsymbol{G} = -(\boldsymbol{C}(\boldsymbol{A} + \boldsymbol{BF})^{-1}\boldsymbol{B})^{-1} \qquad (23)$$

and the design of $\boldsymbol{F}$ can be easily calculated using the Ackermann's formula or the pole placement method [19, 20]

$$u_2(n) = -(\boldsymbol{\rho B})^{-1}\boldsymbol{\rho}((\boldsymbol{A} - \boldsymbol{A}_r)\xi(n) - \boldsymbol{B}_r r(n))$$
$$= \boldsymbol{F}\xi(n) + \boldsymbol{G}r(n) \qquad (24)$$

3 Simulation protocols

To assist the performance of the control algorithm, preload and afterload scenarios are presented. In preload scenario test, the total blood volume (V_{total}) was linearly decreased by 500 ml over a period of 60 s. Here, the model parameters were linearly changed at 30 s and the HF condition was taken as the baseline state. These changes associated with the linear decrease in the reference pump flow from $(4 + 3.4\sin(2\pi t/T + 1.5))$ to $(2.5 + 3.4\sin(2\pi t/T + 1.5))$. Next, at the afterload scenario, the ability of the control algorithm to adjust to more severe circulatory perturbations was evaluated. Here, a sustained severe fall in LV contractility to track the reference pump flow was simulated. The model parameters have been changed linearly at 30 s. These changes include a linear increase in the reference pump flow from $(4 + 3.4\sin(2\pi t/T + 1.5))$ to $(5.5 + 3.4\sin((2\pi t + 1.5)/T))$, R_{sa} (decreased linearly by 20%), V_{total} (increased linearly by 500 ml), E_{lv} and E_{rv} (increased linearly by 15%).

In all scenarios, the model parameters have been changed linearly over the period of 60 s. This period has been chosen to verify the system stability at time instants. For this period, the system has been induced at the middle (30 s) and the simulations are continued for another half of the time. The design parameters of the switching function in (14) are $\rho = [11]$, $\tau T = 0.05$, $\epsilon T = 0.025$ and $\alpha T = 0.5$. The resulting values of $\boldsymbol{F}$ and $\boldsymbol{G}$ are [–0.53 0.0805] and (–408.3333), respectively.

4 Results

4.1 Preload scenario

The simulation results of preload scenario can be shown in Fig. 4. The reduction of V_{total} by 500 ml at 30 s, the controller responds to produce a leftward shift of the LV and RV (right ventricular) pressure volume loops, resulting in decreased LV and RV end-diastolic and end-systolic volumes, as well as end-diastolic and end-systolic pressures as shown in Fig. 4a. Consequently this action, decrease mean pump speed from ~2100 to 1740 rpm and subsequently mean pump flow decreased from 4.7 to 2.8 l/min. In addition, Fig. 4d shows that the simulated pump flow accurately tracks the desired reference flow within an error of ± 0.21 l/min.

4.2 Afterload scenario

The ability of the controller to adjust to longer term circulatory perturbations that were sufficient to track the reference pump flow is illustrated in Fig. 5. In this scenario, LV contractility was linearly decreased at $t = 30$ s, over a period of 10 s. A sustained severe fall in LV contractility produced a rightward shift of the LV pressure volume loops, resulting in increased LV end-diastolic and end-systolic volumes. Peak-systolic LV pressure, as well as stroke volume (SV), were decreased. The large fall in the LVAD flow and associated changes to flow pulsatility is handled initially by a tracking the reference pump flow. It can be observed that the rotational pump speed successfully increases speed from 2900 to 3400 rpm to increase the mean pump flow when the flow falls below the lower limit of 3 l/min. Also, Fig. 5d shows that the simulated pump flow is accurately tracked the desired reference flow within an error of ± 0.22 l/min. Table 1 shows the test results of different hemodynamic variables for the HF condition.

5 Discussion

In general, our physiological control computer simulation studies have demonstrated the feasibility of a non-invasive sensor approach based on accelerometery. The reliability of this signal to represent cardiac preload requires integration with other
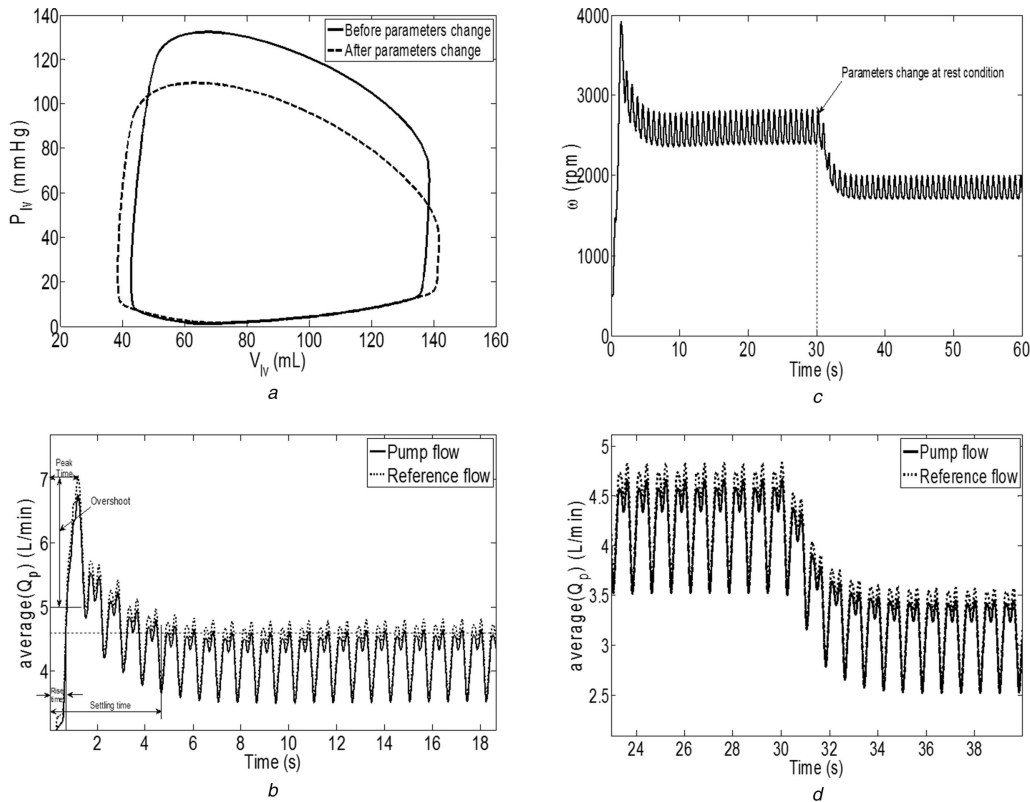
Fig. 4 *Hemodynamic variables results in the preload scenario*
(a) LV volume versus LV pressure before and after parameter change, *(b)* Mean pump rotational speed; ω: pump speed, *(c)* Pump flow compared with desired reference flow at the initial time, *(d)* Pump flow compared with desired reference flow at the induced time
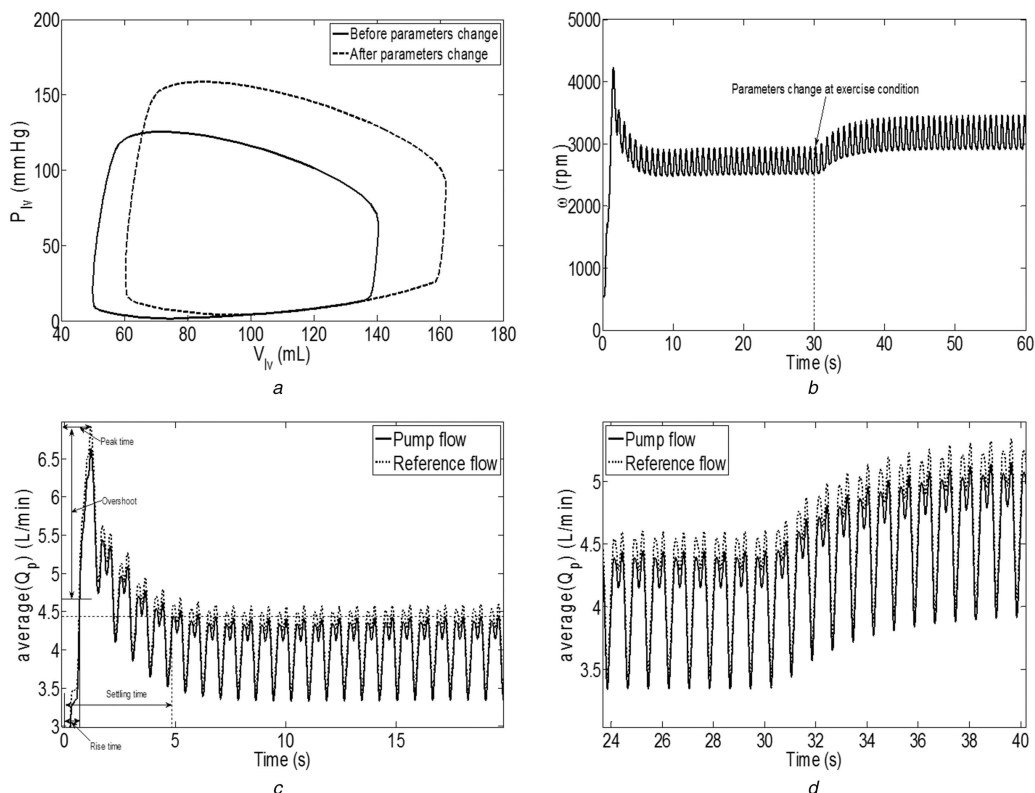

Fig. 5 *Hemodynamic variables results in the afterload scenario*
(a) LV volume versus LV pressure before and after parameter change, *(b)* Mean pump rotational speed; ω: pump speed, *(c)* Pump flow compared with desired reference flow at initial time, *(d)* Pump flow compared with desired reference flow at induced time

physiological signals such as heart rate and respiratory rate. However, HF patients are observed to often have limited changes in these signals. So, we believe that the integration of an invasive pressure sensor may be required to effectively monitor and control

cardiac preload and so give the pump system a natural Frank–Starling behaviour.

In this field, different research groups are designed and implanted valuable physiological algorithms for IRBP output. For instance, Choi *et al.* [12] used a fuzzy logic controller that relied on

IET Syst. Biol., 2018, Vol. 12 Iss. 2, pp. 68-72

71

Table 1 Changes of hemodynamic variables at preload and afterload

Variables		HF + LVAD		
	Units	Normal	Preload	Afterload
LV end diastolic pressure (P_lved)	mmHg	9.50	8.50	21.79
LV end systolic volume (V_lves)	l/min	40.50	39.00	62.00
LV end diastolic volume (V_lved)	l/min	140.70	141.90	152.4
SV	ml	102.00	100.0	100.0
average of actual flow ($\overline{Q}_\text{act}$)	l/min	4.50	3.40	5.05
average of estimated ($\overline{Q}_\text{est}$)	l/min	4.95	3.65	5.52

the pulsatility index as the input to the controller. This index is used to drive the pump at a level that provides maximum possible flow without ventricular suction occurring. The flow is not measured, rather a model of the pump is used to determine the flow, based on pump speed and current. Similarly, Casas *et al.* [21] used a fuzzy Logic controller to maintain pump flow within specific limits. Feedback inputs were pressure difference across pump and the pump speed – a model of the pump flow was used for calculating an estimated pump flow using these variables. However, none of them have achieved the regulation of differential pressure and pump flow at variable speed.

Generally, pump flow pulsatility increases with increasing pump speed once suction occurs [22]. This raises a serious concern with the present control strategy which uses pump flow pulsatility as an input, as it could lead to inappropriate increases in pump speed if suction occurs. A number of measures were suggested to minimise this possibility: (i) introduction of a lower limit for pump flow pulsatility; (ii) proportional and integral gains of the controller were set to allow the controller to respond quickly to a change (i.e. a reduction) in preload to avoid the occurrence of suction; (iii) a suction detection algorithm [12, 23] is implemented to force a change in the pump speed and to produce an alarm if suction is detected. In addition, as with all types of pulsatility control, the present control strategy assumes that the left ventricle has some residual contractility to provide pump flow pulsatility.

In this work, the transient overshoot is a significant issue which can be observed in the first two seconds in Fig. 4*c* at the first scenario and Fig. 5*c* at the second scenario. Despite, the transient response is high at the initial time; the average pump flow stays within the acceptable clinical ranges without any occurrence of over-pumping. Future studies may include other advanced modern control methods such as robust linear quadratic control [24], H-infinity control based robust stabilisation [25], robust controller switching [26], communication-limited control [27].

6 Conclusion

In this work, the innovative of a physiological control algorithm that mimics the metabolic demand of the human body is presented. The immediate response of the controller to short term and longer term of circulatory changes were evaluated. Stability and feasibility of the control system were demonstrated through the tests. Results showed that the present controller allows the LV to automatically adjust to the RV output and reduces the risk of suction.

7 Acknowledgments

8 References

[1] Acker, M.A.: 'Surgical therapies for heart failure', *J. Card. Fail.*, 2004, **10**, (6), pp. S220–S224
[2] Guyton, A.C., Hall, J.E.: '*Textbook of medical physiology*' (Saunders Company, Philadelphia, 1996)
[3] Slaughter, M.S., Rogers, J.G., Milano, C.A., *et al.*: 'Advanced heart failure treated with continuous-flow left ventricular assist device', *N. Engl. J. Med.*, 2009, **361**, (23), pp. 2241–2251
[4] Wu, Y., Allaire, P.E., Tao, G., *et al.*: 'Modeling, estimation, and control of human circulatory system with a left ventricular assist device', *IEEE Trans. Control Syst. Technol.*, 2007, **15**, (4), pp. 754–767
[5] Rose, E.A., Gelijns, A.C., Moskowitz, A.J., *et al.*: 'Long-term use of a left ventricular assist device for end-stage heart failure', *N. Engl. J. Med.*, 2001, **345**, (20), pp. 1435–1443
[6] Salamonsen, R.F., Lim, E., Gaddum, N., *et al.*: 'Theoretical foundations of a starling-like controller for rotary blood pumps', *Artif. Organs*, 2012, **36**, (9), pp. 787–796
[7] Giridharan, G.A., Skliar, M.: 'Physiological control of blood pumps using intrinsic pump parameters: a computer simulation study', *Artif. Organs*, 2006, **30**, (4), pp. 301–307
[8] alamonsen, R.F., Mason, D.G., Ayre, P.J.: 'Response of rotary blood pumps to changes in preload and afterload at a fixed speed setting are unphysiological when compared with the natural heart', *Artif. Organs*, 2011, **35**, (3), pp. E47–E53
[9] Giridharan, G.A., Pantalos, G.M., Gillars, K.J., *et al.*: 'Physiologic control of rotary blood pumps: an in vitro study', *ASAIO J.*, 2004, **50**, (5), pp. 403–409
[10] Frazier, O.H., Shah, N.A., Myers, T.J., *et al.*: 'Use of the flowmaker (Jarvik 2000) left ventricular assist device for destination therapy and bridging to transplantation', *Cardiology*, 2004, **101**, (1-3), pp. 111–116
[11] Wu, Y., Allaire, P.E., Tao, G., *et al.*: 'An advanced physiological controller design for a left ventricular assist device to prevent left ventricular collapse', *Artif. Organs*, 2003, **27**, (10), pp. 926–930
[12] Choi, S., Antaki, J.E., Boston, R., *et al.*: 'A sensorless approach to control of a turbodynamic left ventricular assist system', *IEEE Trans. Control Syst. Technol.*, 2001, **9**, (3), pp. 473–482
[13] Hung, J.Y., Gao, W., Hung, J.C.: 'Variable structure control: a survey', *IEEE Trans. Ind. Electron.*, 1993, **40**, (1), pp. 2–22
[14] Lim, E., Dokos, S., Cloherty, S.L., *et al.*: 'Parameter-optimized model of cardiovascular–rotary blood pump interactions', *IEEE Trans. Biomed. Eng.*, 2010, **57**, (2), pp. 254–266
[15] Bakouri, M.A., Salamonsen, R.F., Savkin, A.V., *et al.*: 'A sliding mode-based starling-like controller for implantable rotary blood pumps', *Artif. Organs*, 2014, **38**, (7), pp. 587–593
[16] Gao, W., Wang, Y., Homaifa, A.: 'Discrete-time variable structure control systems', *IEEE Trans. Ind. Electron.*, 1995, **42**, (2), pp. 117–122
[17] Spurgeon, S.K.: 'Hyperplane design techniques for discrete-time variable structure control systems', *Int. J. Control*, 1992, **55**, (2), pp. 445–456
[18] Strang, G., Borre, K.: '*Linear algebra, geodesy, and GPS*' (Wellesley Cambridge Pr, USA, 1997)
[19] Khalil, H.K., Grizzle, J.W.: '*Nonlinear systems*' (Prentice-Hall, New Jersey, 1996)
[20] Goodwin, G.C., Graebe, S.F., Salgado, M.E.: '*Control system design*' (Prentice-Hall, New Jersey, 2001)
[21] Casas, F., Orozco, A., Smith, W.A., *et al.*: 'A fuzzy system cardio pulmonary bypass rotary blood pump controller', *Expert Syst. Appl.*, 2004, **26**, (3), pp. 357–361
[22] AlOmari, A.H., Savkin, A.V., Stevens, M., *et al.*: 'Developments in control systems for rotary left ventricular assist devices for heart failure patients: a review', *Physiol. Meas.*, 2013, **34**, (1), p. R1
[23] Mason, D.G., Hilton, A.K., Salamonsen, R.F.: 'Reliable suction detection for patients with rotary blood pumps', *ASAIO J.*, 2008, **54**, (4), pp. 359–366
[24] Savkin, A.V., Petersen, I.R.: 'Minimax optimal control of uncertain systems with structured uncertainty', *Int. J. Robust Nonlinear Control*, 1995, **5**, (2), pp. 119–137
[25] Petersen, I.R., Ugrinovskii, V.A., Savkin, A.V.: '*Robust control design using H∞ methods*' (Springer, London, 2000)
[26] Savkin, A.V., Skafidas, E., Evans, R.J.: 'Robust output feedback stabilizability via controller switching', *Automatica*, 1999, **35**, (1), pp. 69–74
[27] Savkin, A.V., Cheng, T.M.: 'Detectability and output feedback stabilizability of nonlinear networked control systems', *IEEE Trans. Autom. Control*, 2007, **52**, (4), pp. 730–735